The PVLAS experiment: detecting vacuum magnetic birefringence

G Zavattini[3], F Della Valle[1], U Gastaldi[2], G Messineo[3], E Milotti[1], R Pengo[2], L Piemontese[4] and G Ruoso[2]

[1] INFN, Sez. di Trieste and Dip. di Fisica, Università di Trieste, via A. Valerio 2, I-34127 Trieste, Italy
[2] INFN, Lab. Naz. di Legnaro, viale dell'Università 2, I-35020 Legnaro, Italy
[3] INFN, Sez. di Ferrara and Dip. di Fisica e di Scienze della Terra, Università di Ferrara, via Saragat 1, Edificio C, I-44122 Ferrara, Italy
[4] INFN, Sez. di Ferrara, via Saragat 1, Edificio C, I-44122 Ferrara, Italy

E-mail: guido.zavattini@unife.it

Abstract. The PVLAS collaboration is presently assembling a new apparatus to detect vacuum magnetic birefringence. This property is related to the structure of the QED vacuum and is predicted by the Euler-Heisenberg-Weisskopf effective Lagrangian. It can be detected by measuring the ellipticity acquired by a linearly polarised light beam propagating through a strong magnetic field. Here we report results of a scaled-down test setup and briefly describe the new PVLAS apparatus. This latter one is in construction and is based on a high-sensitivity ellipsometer with a high-finesse Fabry-Perot cavity ($> 4\times10^5$) and two 0.8 m long 2.5 T rotating permanent dipole magnets. Measurements with the test setup have improved by a factor 2 the previous upper bound on the parameter A_e, which determines the strength of the nonlinear terms in the QED Lagrangian: $A_e^{(\mathrm{PVLAS})} < 3.3\times10^{-21}$ T^{-2} 95% c.l.

1. Introduction

In the absence of matter, Maxwell's equations can be obtained from the classical electromagnetic Lagrangian density $\mathcal{L}_{\mathrm{Cl}}$ (in S.I. units)

$$\mathcal{L}_{\mathrm{Cl}} = \frac{1}{2\mu_0}\left(\frac{E^2}{c^2} - B^2\right) \tag{1}$$

where μ_0 is the magnetic permeability of vacuum and c is the speed of light in vacuum. A quadratic Lagrangian leads to linear partial differential equations for the fields, and the superposition principle holds, thereby excluding light-light scattering and other non linear electromagnetic effects in vacuum.

With the introduction of Dirac's equation (1928) for electrons and Heisenberg's Uncertainty Principle (1927), Euler, Heisenberg and Weisskopf in 1936 [1] derived an effective Lagrangian density which leads to electromagnetic non linear effects even in vacuum. For photon energies well below the electron mass and fields much smaller than their critical values, $B \ll B_{\mathrm{crit}} = m_e^2c^2/e\hbar = 4.4\times10^9$ T, $E \ll E_{\mathrm{crit}} = m_e^2c^3/e\hbar = 1.3\times10^{18}$ V/m, the Euler-Heisenberg-Weisskopf

effective Lagrangian can be written as

$$\mathcal{L}_{\rm EHW} = \mathcal{L}_{\rm Cl} + \frac{A_e}{\mu_0}\left[\left(\frac{E^2}{c^2} - B^2\right)^2 + 7\left(\frac{\vec{E}}{c}\cdot\vec{B}\right)^2\right] \tag{2}$$

where

$$A_e = \frac{2}{45\mu_0}\frac{\alpha^2\lambda\!\!\!^{-3}_e}{m_e c^2} = 1.32\times10^{-24}\ \mathrm{T}^{-2} \tag{3}$$

with $\lambda\!\!\!^{-}_e = \hbar/mc$ being the Compton wavelength of the electron, $\alpha = e^2/(\hbar c 4\pi\epsilon_0)$ the fine structure constant, m_e the electron mass.

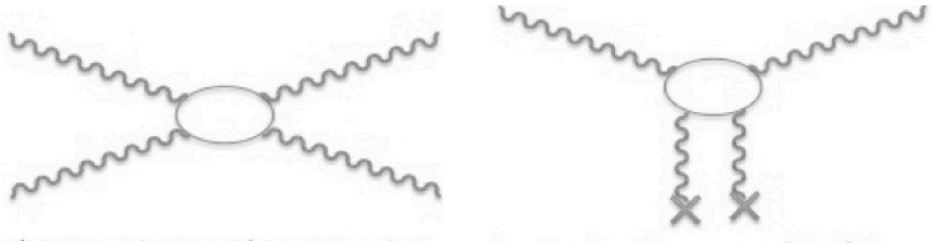

a) b)

Figure 1. Feynman diagrams for four electromagnetic field interactions. Left: elastic photon-photon scattering. Right: Vacuum magnetic birefringence

This Euler-Heisenberg-Weisskopf Lagrangian allows four field interactions that can be represented, to first order, by the Feynman diagrams shown in Figure 1 a) and b). Figure 1 a) represents light by light scattering whereas Figure 1 b) represents the interaction of real photons with a classical field leading to vacuum magnetic birefringence. Quantum Electrodynamics (QED) also predicts non-linear effects in vacuum leading to the same birefringence and light-by-light (LbL) scattering as the Euler-Heisenberg Lagrangian through the four-photons box diagram [2, 3, 4, 5, 6, 7, 8, 9].

Vacuum magnetic linear birefringence and light-light interaction in vacuum at very low energies have yet to be observed. Several experimental efforts are underway to detect such effects [10, 11, 12, 13, 14, 15, 16, 17, 18, 19]. Before the measurements presented here (and in [20]), the previous bound on four photon interaction was set by the PVLAS collaboration [12] with an upper bound on vacuum magnetic birefringence $\Delta n^{(\rm PVLAS)}$ measured with a magnetic field $B = 2.3$ T

$$\Delta n^{(\rm PVLAS)} < 1.0\times10^{-19} \qquad @\ 2.3\ \mathrm{T\ and\ 95\%\ c.l.} \tag{4}$$

The measurement was performed at $\lambda = 1064$ nm, corresponding to a photon energy $\hbar\omega = 1.17$ eV. This limit translates into an upper bound for the unpolarised photon-photon elastic cross section [5, 6, 7, 8, 9] as

$$\sigma^{(\rm PVLAS)}_{\gamma\gamma}(1.17\ \mathrm{eV}) < 4.6\times10^{-62}\ \mathrm{m}^2. \tag{5}$$

The predicted QED value of the vacuum magnetic birefringence (see below) $\Delta n^{(\rm EHW)}$ and photon-photon elastic scattering cross section $\sigma^{(\rm EHW)}_{\gamma\gamma}$ are

$$\Delta n^{(\rm EHW)} = 2.1\times10^{-23} \qquad @\ 2.3\ \mathrm{T} \tag{6}$$

$$\sigma^{(\rm EHW)}_{\gamma\gamma}(1.17\ \mathrm{eV}) = 1.8\times10^{-69}\ \mathrm{m}^2 \tag{7}$$

1.1. Electrodynamics
To calculate the magnetic birefringence of vacuum one can proceed by determining the electric displacement vector $\vec{D}$ and the magnetic intensity vector $\vec{H}$ from the Lagrangian density $\mathcal{L}_{\mathrm{EHW}}$ of Eq. (2) by using the constitutive relations [3]

$$\vec{D} = \frac{\partial \mathcal{L}}{\partial \vec{E}} \quad \text{and} \quad \vec{H} = -\frac{\partial \mathcal{L}}{\partial \vec{B}}. \tag{8}$$

From these one obtains

$$\vec{D} = \epsilon_0 \vec{E} + \epsilon_0 A_e \Big[4\Big(\frac{E^2}{c^2} - B^2\Big)\vec{E} + 14\Big(\vec{E}\cdot\vec{B}\Big)\vec{B}\Big] \tag{9}$$

$$\vec{H} = \frac{\vec{B}}{\mu_0} + \frac{A_e}{\mu_0}\Big[4\Big(\frac{E^2}{c^2} - B^2\Big)\vec{B} - 14\Big(\frac{\vec{E}}{c}\cdot\vec{B}\Big)\frac{\vec{E}}{c}\Big]. \tag{10}$$

Let's consider a linearly polarised beam of light propagating perpendicularly to an external magnetic field $\vec{B}_{\mathrm{ext}}$. With $\vec{D}$ and $\vec{H}$, and using Maxwell's equations in media, one can describe light propagation in an external field. It is evident that the equations for light propagation will no longer be linear due to the non linear dependence of $\vec{D}$ and $\vec{H}$ on $\vec{E}$ and $\vec{B}$, respectively. We therefore substitute $\vec{E} = \vec{E}_\gamma$ and $\vec{B} = \vec{B}_\gamma + \vec{B}_{\mathrm{ext}}$ in (9) and (10), where the index γ refers to the light, assuming $|\vec{B}_{\mathrm{ext}}| \gg |\vec{B}_\gamma|$. One finds the following relations for the relative dielectric constant and magnetic permeability of vacuum:

$$\begin{cases} \epsilon_{\parallel}^{(\mathrm{EHW})} = 1 + 10 A_e B_{\mathrm{ext}}^2 \\ \mu_{\parallel}^{(\mathrm{EHW})} = 1 + 4 A_e B_{\mathrm{ext}}^2 \\ n_{\parallel}^{(\mathrm{EHW})} = 1 + 7 A_e B_{\mathrm{ext}}^2 \end{cases} \qquad \begin{cases} \epsilon_{\perp}^{(\mathrm{EHW})} = 1 - 4 A_e B_{\mathrm{ext}}^2 \\ \mu_{\perp}^{(\mathrm{EHW})} = 1 + 12 A_e B_{\mathrm{ext}}^2 \\ n_{\perp}^{(\mathrm{EHW})} = 1 + 4 A_e B_{\mathrm{ext}}^2 \end{cases} \tag{11}$$

where the indices $\parallel$ and $\perp$ refer to light polarisation parallel and perpendicular to $\vec{B}_{\mathrm{ext}}$, respectively.

From these sets of equations two important consequences are apparent: the velocity of light in the presence of an external magnetic field is no longer c and vacuum is birefringent with

$$\Delta n^{(\mathrm{EHW})} = n_{\parallel}^{(\mathrm{EHW})} - n_{\perp}^{(\mathrm{EHW})} = 3 A_e B_{\mathrm{ext}}^2. \tag{12}$$

Magnetised vacuum behaves like a uniaxial crystal. Numerically this leads to the value given in equation (6).

2. Experimental method

A birefringence Δn induces an ellipticity ψ on a linearly polarised beam of light given by

$$\psi(\vartheta) = \frac{\Delta\varphi}{2}\sin 2\vartheta = \pi\frac{L\Delta n}{\lambda}\sin 2\vartheta \tag{13}$$

where L is the optical path length within the birefringent region, λ is the wavelength of the light traversing it and ϑ is the angle between the light polarisation and the slow axis, defined in our case by the magnetic field direction. The optical path length through a region of length L can be increased by using a Fabry-Perot cavity; in this case we think of an effective path length L_{eff} and use a capital letter Ψ to indicate the total induced ellipticity. In fact, given a birefringent region of length L within a Fabry-Perot cavity of finesse $\mathcal{F}$, the effective path length is $L_{\mathrm{eff}} = (2\mathcal{F}/\pi)L$. Today finesses $\mathcal{F} > 400000$ can be obtained.

In the Euler-Heisenberg-Weisskopf case which we are discussing here, Δn depends quadratically on the magnetic field $\vec{B}$. High magnetic fields can be obtained with superconducting magnets but, as we will see below, it is desirable to have a time dependent field either by modulating its intensity, thereby changing Δn, or by rotating the field direction, thereby changing ϑ. This makes superconducting magnets far less appealing than permanent magnets which, today, can reach fields above 2.5 T. In the BFRT (Brookhaven, Fermilab, Rochester, Trieste) experiment the first scheme was adopted [21] by ramping the field intensity, whereas PVLAS chose to rotate an entire superconducting magnet [10, 11, 12] thereby rotating the magnetic field direction. At present the PVLAS collaboration has abandoned the superconducting magnet for 2.5 T permanent dipole magnets which are relatively inexpensive, have no running costs and have in principle 100% duty cycle, allowing very long integration times.

We are working with a Nd:YAG laser emitting radiation at 1064 nm. Frequency doubled versions exist and could double the induced ellipticity, but at the moment the highest finesses have been obtained for infrared light.

The expected ellipticity must be extracted from the noise within the maximum available integration time. For this reason, the magnetic field is made time dependent, to move away from DC and limit $1/f$ noise. Homodyne and heterodyne detections are two possible schemes. This second technique has been adopted in the PVLAS apparatus.

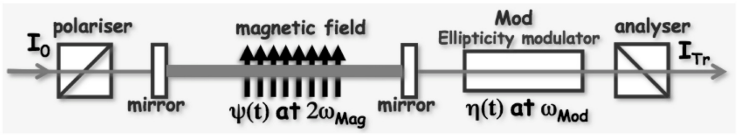

Figure 2. Scheme of the PVLAS ellipsometer.

A scheme of the PVLAS ellipsometer is shown in Figure 2. The input polariser linearly polarises the laser beam of intensity I_0 which then enters the sensitive region delimited by the Fabry-Perot cavity mirrors where the magnetic field is present. The laser is phase locked to this cavity. After the cavity the laser beam passes through an ellipticity modulator which adds a known time dependent ellipticity $\eta(t)$ to the beam. This modulator ellipticity adds to the ellipticity $\Psi(t)$ acquired within the magnetic field region. After the modulator, the beam passes through the analyser which selects the polarisation perpendicular to the input polarisation and finally a photodiode detects $I_{\rm Tr}$. The sought for information can be extracted from the Fourier spectrum of $I_{\rm Tr}$ and from the value of the intensity $I_{\rm out}$ before the analyser.

2.1. Estimate of the effect

To better understand what follows, it is useful to present some numerical values of the different quantities involved in the PVLAS experiment. Considering the vacuum magnetic birefringence due to the Euler-Heisenberg-Weisskopf Lagrangian, let us determine the ellipticity we expect in the apparatus under construction. The magnets have a total magnetic field length $L = 1.6$ m with a measured field intensity $|\vec{B}_{\rm ext}| = 2.5$ T resulting in $\int B^2_{\rm ext}\, dL = 10$ T^{2}m. In the estimate we use the the maximum finesse value we have reached: $\mathcal{F} = 414000$ [22]. Putting these numbers together leads to

$$\Psi_{\rm PVLAS} = 2\mathcal{F}\,\frac{3A_e \int B^2_{\rm ext}\, dL}{\lambda} = 3 \times 10^{-11}. \qquad (14)$$

Assuming a maximum integration time $T_{\max} = 10^6$ s and a signal to noise ratio SNR = 1 implies that the sensitivity must be

$$s_{\mathrm{PVLAS}} < \Psi_{\mathrm{PVLAS}}\sqrt{T_{\max}} = 3 \times 10^{-8}\ \mathrm{Hz}^{-1/2}. \tag{15}$$

In principle this is well above the shot noise limit (see formula (27) below). Unfortunately, as will be briefly discussed below, other noise sources are present which limit the ellipsometer sensitivity. We now discuss in detail various issues of the measurement technique and of the setup.

2.2. Heterodyne technique and optical path multiplier

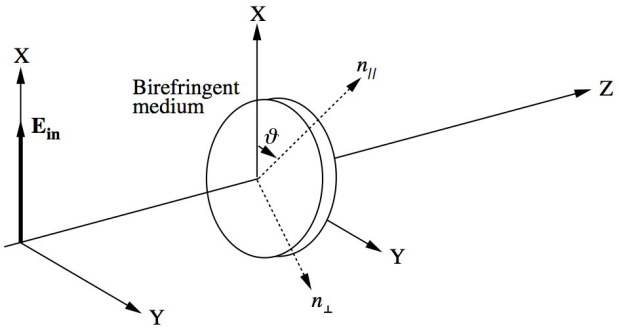

Figure 3. Reference frame for the calculations using the Jones matrix formalism. The birefringent medium has a thickness L.

Considering the coherence of the light source, a full treatment of the system can be done with the Jones matrix formalism [23]. For the purpose of our discussion let the laser beam propagate along the Z axis and let the incoming (linear) polarisation define the X axis (Figure 3). The Jones matrix for a uniaxial birefringent element of thickness L is given by

$$\mathbf{BRF}(\vartheta) = \begin{pmatrix} 1 + \imath\psi\cos 2\vartheta & \imath\psi\sin 2\vartheta \\ \imath\psi\sin 2\vartheta & 1 - \imath\psi\cos 2\vartheta \end{pmatrix} \tag{16}$$

where $\psi = \Delta\varphi/2$ ($\psi \ll 1$) is now the maximum ellipticity acquired by the light and ϑ represents the angle between the slow axis ($n_{\parallel} > n_{\perp}$) of the medium and the X axis.

In the heterodyne technique an ellipticity modulator is introduced after the birefringent region (in our case a Photoelastic Modulator, PEM), which adds a known sinusoidal ellipticity $\eta(t)$. This results in the linearisation of ψ in the intensity signal. In fact, the Jones matrix for the modulator is the same as **BRF** with ϑ set at an angle of $\pi/4$ ($\psi \ll \eta \ll 1$):

$$\mathbf{MOD} = \begin{pmatrix} 1 & \imath\eta(t) \\ \imath\eta(t) & 1 \end{pmatrix}. \tag{17}$$

Given an input electric field vector $\vec{E}_{\mathrm{in}} = E_0\binom{1}{0}$ the resulting vector describing the electric field after the modulator will be

$$\vec{E}_{\mathrm{Tr}} = E_0 \cdot \mathbf{MOD} \cdot \mathbf{BRF} \cdot \begin{pmatrix} 1 \\ 0 \end{pmatrix} = E_0 \begin{pmatrix} 1 + \imath\psi\cos 2\vartheta - \eta(t)\psi\sin 2\vartheta \\ \imath\eta(t) + \imath\psi\sin 2\vartheta - \eta(t)\psi\cos 2\vartheta \end{pmatrix}. \tag{18}$$

Neglecting second order terms, the intensity $I_{\rm Tr}$ after the analyser will be

$$I_{\rm Tr}(t) = I_0 \left|\imath\eta(t) + \imath\psi \sin 2\vartheta\right|^2 \simeq I_0 \left[\eta(t)^2 + 2\eta(t)\psi \sin 2\vartheta\right] \tag{19}$$

which now depends linearly on the ellipticity ψ.

To further improve the sensitivity of the ellipsometer one can increase the number of passes through the birefringent region. Either a multi-pass cavity or a Fabry-Perot cavity can be used for this purpose. In the PVLAS experiment a Fabry-Perot has been chosen. Let $\mathcal{T}$ and $\mathcal{R}$ be the transmittivity and reflectivity of the Fabry-Perot mirrors, and p their losses such that $\mathcal{T} + \mathcal{R} + p = 1$. In this case it can be shown that the electric field vector after the analyser is

$$\vec{E}_{\rm Tr} = E_0 \frac{\mathcal{T}}{\mathcal{T}+p} \begin{pmatrix} 0 \\ \\ \imath\eta(t) + \imath\left(\dfrac{1+\mathcal{R}}{1-\mathcal{R}}\right)\psi \sin 2\vartheta \end{pmatrix} \tag{20}$$

and, indicating the output intensity, including mirror losses, as $I_{\rm out} = \left(E_0 \frac{\mathcal{T}}{\mathcal{T}+p}\right)^2$, the detected intensity will be

$$I_{\rm Tr}(t) = I_{\rm out}\left|\imath\eta(t) + \imath\left(\frac{1+\mathcal{R}}{1-\mathcal{R}}\right)\psi \sin 2\vartheta\right|^2. \tag{21}$$

The ellipticity ψ is multiplied by a factor $\frac{1+\mathcal{R}}{1-\mathcal{R}} \approx 2\mathcal{F}/\pi$ (typically $\mathcal{R} \approx 99.999\%$) where $\mathcal{F}$ is defined as the finesse of the Fabry-Perot. To complete the discussion, one finds experimentally that static and slowly varying ellipticities, indicated as $\alpha(t)$, are always present in a real apparatus and that two crossed polarisers have an intrinsic extinction ratio σ^2, mainly due to imperfections in the calcite crystals. Therefore, taking into account an additional spurious ellipticity term $\alpha(t)$ (since $\alpha, \psi, \eta \ll 1$ these terms commute and therefore add up algebraically) and a term proportional to σ^2, the total intensity at the output of the analyser will be

$$\begin{aligned} I_{\rm Tr}(t) &= I_{\rm out}\left[\sigma^2 + \left|\imath\eta(t) + \imath\left(\frac{2\mathcal{F}}{\pi}\right)\psi \sin 2\vartheta + \imath\alpha(t)\right|^2\right] \simeq \\ &\simeq I_{\rm out}\left[\sigma^2 + \eta(t)^2 + \alpha(t)^2 + 2\eta(t)\left(\frac{2\mathcal{F}}{\pi}\right)\psi \sin 2\vartheta + 2\eta(t)\alpha(t)\right]. \end{aligned} \tag{22}$$

In PVLAS, to be able to distinguish the large term $\eta(t)\alpha(t)$ from the term $\eta(t)\left(\frac{2\mathcal{F}}{\pi}\right)\psi \sin 2\vartheta$, $\psi \sin 2\vartheta$ is also modulated in time by rotating the magnetic field direction (varying ϑ). The final expression, explicitly indicating the time dependence of ϑ, for the intensity at the output of the analyser is therefore

$$I_{\rm Tr}(t) = I_{\rm out}\left[\sigma^2 + \eta(t)^2 + \alpha(t)^2 + 2\eta(t)\left(\frac{2\mathcal{F}}{\pi}\right)\psi \sin 2\vartheta(t) + 2\eta(t)\alpha(t)\right]. \tag{23}$$

This expression is at the basis of the ellipsometer in the PVLAS apparatus [24]. Small ellipticities add up algebraically and the Fabry-Perot multiplies the single pass ellipticity $\psi \sin 2\vartheta$, generated within the cavity, by a factor $(1+\mathcal{R})/(1-\mathcal{R}) \approx 2\mathcal{F}/\pi$, where $\mathcal{F}$ is the finesse of the cavity. The ellipticity signal to be detected is therefore $\Psi(\vartheta) = (2\mathcal{F}/\pi)\psi \sin 2\vartheta$.

The Fabry-Perot as an optical path amplifier works well until the accumulated phase difference due to birefringences within the cavity is less than $\pi/2$. Beyond this value the interferometer has two separate resonances for two orthogonal polarisations [24] and therefore elliptically polarised light cannot be resonant. As total birefringences also include the intrinsic birefringence of the cavity mirrors, two mirrors with similar characteristics must be used and their birefringence axes aligned.

2.3. Fourier components
In the PVLAS experiment, $\eta(t) = \eta_0 \cos(2\pi\nu_{\rm Mod}t + \theta_{\rm Mod})$ and the magnetic field direction is rotated at a frequency $\nu_{\rm Mag}$: $\vartheta(t) = 2\pi\nu_{\rm Mag}t + \vartheta_{\rm Mag}$. A Fourier analysis of the intensity $I_{\rm Tr}(t)$ of equation (21) results in four main frequency components each with a definite amplitude and phase. These are reported in table 1.

Table 1. Intensity of the frequency components of the signal after the analyser.

Frequency	Fourier component	$I_{\rm Tr}/I_{\rm out}$	Phase
dc	$I_{\rm dc}$	$\sigma^2 + \alpha_{\rm dc}^2 + \eta_0^2/2$	$-$
$\nu_{\rm Mod}$	$I_{\nu_{\rm Mod}}$	$2\alpha_{\rm dc}\eta_0$	$\theta_{\rm Mod}$
$\nu_{\rm Mod} \pm 2\nu_{\rm Mag}$	$I_{\nu_{\rm Mod}\pm 2\nu_{\rm Mag}}$	$\eta_0 \dfrac{2\mathcal{F}}{\pi}\psi$	$\theta_{\rm Mod} \pm 2\vartheta_{\rm Mag}$
$2\nu_{\rm Mod}$	$I_{2\nu_{\rm Mod}}$	$\eta_0^2/2$	$2\theta_{\rm Mod}$

The presence of a component at $\nu_{\rm Mod} \pm 2\nu_{\rm Mag}$ in the signal identifies an ellipticity induced by the rotating magnetic field. Furthermore the phase of this component must satisfy the value in table 1. In the presence of a signal above background with the correct Fourier phase, the ellipticity $\Psi = (2\mathcal{F}/\pi)\psi$ can be calculated from $I_{\rm out}$, from the Fourier components $I_{\nu_{\rm Mod}\pm 2\nu_{\rm Mag}}$, and from $I_{2\nu_{\rm Mod}}$ as the average of the two sideband signals:

$$\Psi = \frac{1}{2}\left(\frac{I_{\nu_{\rm Mod}+2\nu_{\rm Mag}}}{\sqrt{2I_{\rm out}I_{2\nu_{\rm Mod}}}} + \frac{I_{\nu_{\rm Mod}-2\nu_{\rm Mag}}}{\sqrt{2I_{\rm out}I_{2\nu_{\rm Mod}}}}\right). \tag{24}$$

2.4. Noise considerations
Indicating with $R_{\nu_{\rm Mod}\pm 2\nu_{\rm Mag}}$ the peak (as opposed to rms) noise spectral density at the signal frequencies, and assuming $R_{\nu_{\rm Mod}+2\nu_{\rm Mag}} = R_{\nu_{\rm Mod}-2\nu_{\rm Mag}}$ but uncorrelated, the sensitivity spectral density s of the ellipsometer for a unity signal to noise ratio is

$$s = \frac{1}{2}\frac{\sqrt{R^2_{\nu_{\rm Mod}+2\nu_{\rm Mag}} + R^2_{\nu_{\rm Mod}-2\nu_{\rm Mag}}}}{\sqrt{2I_{\rm out}I_{2\nu_{\rm Mod}}}} = \frac{1}{\sqrt{2}}\frac{R_{\nu_{\rm Mod}+2\nu_{\rm Mag}}}{\sqrt{2I_{\rm out}I_{2\nu_{\rm Mod}}}}. \tag{25}$$

In principle, the noise limit for such a system is determined by the rms shot noise $i_{\rm shot}$ of the current $i_{\rm dc}$:

$$i_{\rm shot} = \sqrt{2ei_{\rm dc}\Delta\nu} = \sqrt{2eI_{\rm out}q\left(\sigma^2 + \frac{\eta_0^2}{2} + \alpha_{\rm dc}^2\right)\Delta\nu} \tag{26}$$

where q is the efficiency of the photodetector, and $\Delta\nu$ the bandwidth. In the case $\eta_0^2 \gg \sigma^2, \alpha_{\rm dc}^2$, the dc current will depend only on η_0. By substituting $R_{\nu_{\rm Mod}+2\nu_{\rm Mag}} = \sqrt{2}\ i_{\rm rms}/(q\sqrt{\Delta\nu})$ with $i_{\rm rms} = i_{\rm shot}$ into Eq. (25), the peak shot-noise sensitivity spectral density $s_{\rm shot}$ becomes

$$s_{\rm shot} = \sqrt{\frac{e}{I_{\rm out}q}}. \tag{27}$$

Assuming an intensity $I_{\rm out} = 5$ mW and the efficiency of the diode $q = 0.7$ A/W, equation above gives $s_{\rm shot} \sim 7 \times 10^{-9}$ Hz$^{-1/2}$.

Other intrinsic noise sources are rms photodiode dark current noise $i_{\rm dark} = V_{\rm dark}\sqrt{\Delta\nu}/G$ where $V_{\rm dark}$ is the measured rms voltage noise spectral density and G is the transimpedance gain of the photodetection system, Johnson rms current noise in the transimpedance resistor

in the amplifier of the photodiode $i_{\rm J} = \sqrt{4k_BT\Delta\nu/G}$, and relative laser intensity current noise $i_{\rm RIN} = I_{\rm Tr}\, q\, {\rm RIN}(\nu)\sqrt{\Delta\nu}$, where ${\rm RIN}(\nu)$ is the rms relative amplitude noise spectral density of the laser light. These noises must be kept below $i_{\rm shot}$ at a frequency near $\nu_{\rm Mod}$ in order to reach the theoretical sensitivity. Complete expressions for these noise contributions to the ellipticity peak spectral noise density can be obtained from Eq. (25) as functions of the modulation amplitude η_0:

$$s_{\rm shot} = \sqrt{\frac{2e}{I_{\rm out}q}\left(\frac{\sigma^2+\eta_0^2/2}{\eta_0^2}\right)} \tag{28}$$

$$s_{\rm dark} = \frac{V_{\rm dark}}{G}\,\frac{1}{I_{\rm out}\,q\,\eta_0} \tag{29}$$

$$s_{\rm J} = \sqrt{\frac{4k_BT}{G}}\,\frac{1}{I_{\rm out}\,q\,\eta_0} \tag{30}$$

$$s_{\rm RIN} = {\rm RIN}(\nu_{\rm Mod})\,\frac{\sqrt{(\sigma^2+\eta_0^2/2)^2+(\eta_0^2/2)^2}}{\eta_0}. \tag{31}$$

3. Experimental studies

3.1. PVLAS - LNL: main features and limitations

The previous PVLAS apparatus was set up at LNL in Legnaro, Italy and took data from 2002 to 2007. It featured a vertical assembly of the ellipsometer with a 6 m long Fabry-Perot cavity, the injection and detection optics installed on different optical benches resting on the ground and on the top of a granite tower nearly 8 m high, respectively. A superconductive dipole magnet about 1 m long, installed in a cryostat resting on a turntable, provided a rotating magnetic field orthogonal to the light path in the Fabry-Perot cavity. The magnet was operated with magnetic fields up to 5.5 T. The magnet support and the optics tower had different foundations, and were hence mechanically decoupled. Although this apparatus has set best limits on magnetic vacuum birefringence and photon-photon elastic scattering at low energies [12], it suffered from several limitations:

- high stray field when operating the superconducting magnet above 2.3 T, due to saturation of the iron return yoke;
- limited running time due to liquid Helium consumption;
- high running costs for liquid Helium;
- the granite tower could not be seismically insulated, due to its size and configuration;
- with a single magnet, a zero ellipticity measurement was only possible with field off, hence not in the same experimental condition as in the magnetic birefringence measurements.

To solve the first three problems, we have now chosen to work with permanent magnets instead of superconducting ones. In permanent magnets the stray field can be made much smaller and the duty cycle can be as high as 100%. Seismic noise also limited the sensitivity of the LNL setup; instead, a large improvement of this parameter can be obtained by installing the whole ellipsometer on a single seismically isolated optical bench, as shown in ref. [22]. The last point in the list above is extensively addressed in a separate section.

A completely new setup has been designed according to these lines and is being installed in a clean room of the Ferrara section of INFN. The new set up is built using a single 4.8 m long granite optical bench actively isolated, two identical rotating permanent dipole magnets in Halbach configuration, each 0.8 m in length with magnetic field strength $B = 2.5$ T and 2 cm bore. The design of the magnets features an integrated magnetic field shield strongly reducing

the stray field. We plan to rotate them at $\nu_{\rm Mag} = 10$ Hz, thanks to their reduced mass and good balancing. The optical setup features a 2 W tuneable Nd:YAG laser frequency-locked to a 3.2 m long Fabry-Perot cavity using a modified Pound-Drever-Hall scheme [25] and an entirely non magnetic optomechanical setup. The motion of the in-vacuum optical elements is based on stepper piezo motors which maintain their position when powered off and are non magnetic. The whole ellipsometer is kept in a vacuum chamber pumped with non evaporable getters, which are intrinsically non magnetic. Two 1 m long glass tubes traverse the bore of the magnets; each tube is pumped at both ends.

3.2. Two magnet configuration
As reported in ref. [11], the rotating stray magnetic field and the vibrations associated to the masses in rotation can act on the optics and fake ellipticity signals. It is therefore desirable to perform measurements of the zero of the ellipticity scale in conditions as close as possible to those in which an authentic signal is expected. This was not possible in the PVLAS - LNL setup with one single superconducting magnet because when there is no field in the magnet bore also the stray field is absent. A similar problem exists when using a single rotating permanent magnet: the field cannot be turned off. By using two identical magnets and orienting their fields at 90° the net ellipticity generated by the magnetic birefringence is zero. Running the system with the magnets parallel and perpendicular will allow the identification of a real physical signal with respect to some spurious signal due to stray field.

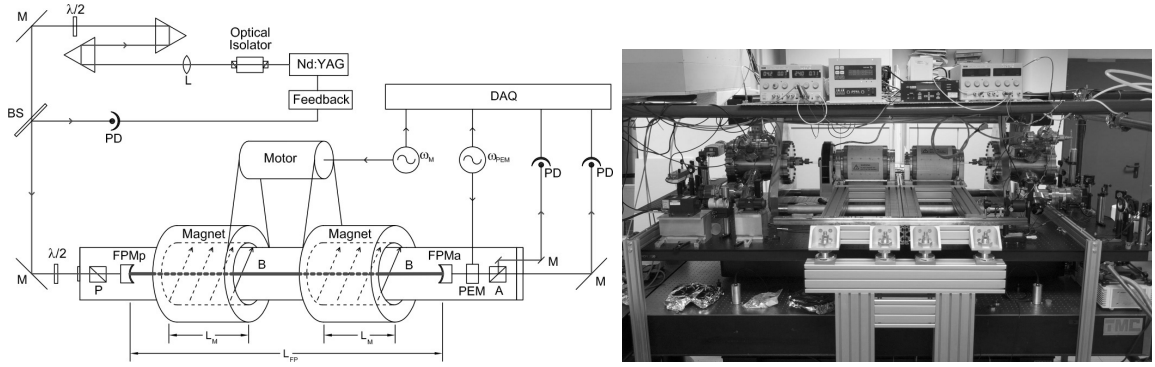

Figure 4. Optical scheme (left panel) and photograph (right panel) of the test apparatus in Ferrara. At the centre one can see the two dipole permanent magnets. The optics is supported by antivibration stages whereas the magnet supports are on the floor.

3.3. Vacuum ellipticity measurements with the test setup
With the test setup (Figure 4), featuring two small magnets, measurements have been performed to understand its limits and optimise the new apparatus in construction. Two different noise sources exist and are under study: wide-band noise and spurious signals at the magnet rotation frequency and its harmonics. Below we briefly report some results in the two cases.

3.3.1. Sensitivity - wide-band noise Noise measurements were first performed without the Fabry-Perot cavity. In this configuration we successfully excluded noise sources from readout electronics and optical elements other than the cavity mirrors, practically reaching the expected sensitivity of $s_{\rm no\ cavity} = 6 \times 10^{-9}$ Hz$^{-1/2}$, dominated by $s_{\rm RIN}$, and a noise floor of $\Psi_{\rm floor} = 1.5 \times 10^{-10}$ with 1600 s integration time.

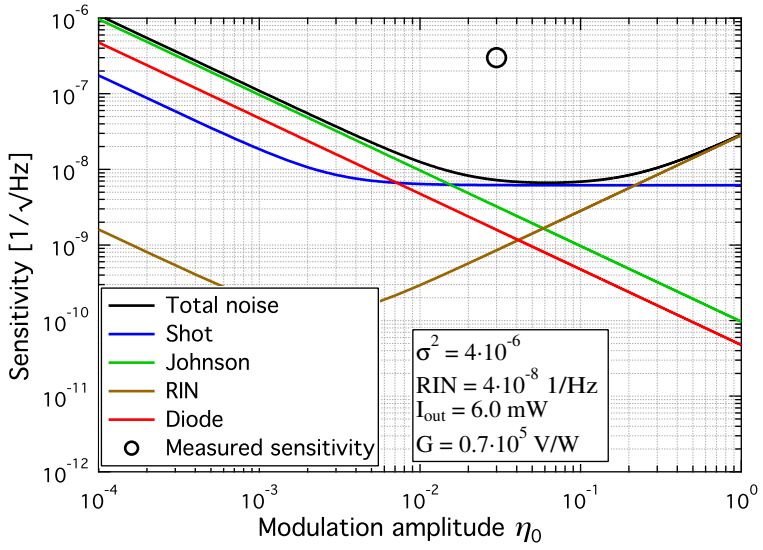

Figure 5. Calculated noise contributions for the PVLAS test apparatus (solid curves). The green curve is the Johnson noise contribution from the transimpedance resistor in the current to voltage converter, the red curve is the dark current noise contribution from the photodiode, the blue curve is the shot noise contribution and the brown curve is the relative intensity noise contribution measured at the output of the cavity. The circle represents the measured ellipticity sensitivity of the apparatus.

With the introduction of a cavity with finesse $\mathcal{F} = 240000$ the noise increased to $s_{\text{cavity}} = 3 \times 10^{-7}$ Hz$^{-1/2}$ at about 6 Hz. This was significantly more than what was expected from the reduction of I_{out} due to cavity losses (see Eq. (27)). The actual ellipticity noise budget situation is depicted in Figure 5 as a function of the modulation amplitude η_0 [12]; in the figure, Relative Intensity Noise (RIN), Johnson noise in the amplifier transimpedance, intrinsic current noise in the photodiode and shot noise are summed quadratically. The circle marks the observed noise level. This unexplained noise is under study and we suspect variations of the intrinsic birefringence of the mirrors.

We also observed that the magnet rotation did not contribute to the wide-band noise, indicating a good isolation between the magnet support and the optical setup.

3.3.2. Spurious peaks With the magnets in rotation we often observe ellipticity peaks varying from a few 10^{-8} to a few 10^{-7} whereas sometimes such peaks are not present. The frequencies of these peaks are at harmonics of the magnet rotation frequency. The variability of these peaks from one run to another seems to depend (in a non reproducible way) on the adjustment of the input and output polarisers which is done with motorised stages. To study the dependence of such peaks on the magnet orientation, a field probe is present near the output side magnet. Changing the relative orientation of the two magnets does not change the amplitude of these peaks but does change their phase; the result of this study indicates that the more sensitive part of the apparatus is the entrance optics. All the motorised stages have small electric motors which might couple to the rotating stray magnetic field and may introduce beam jitter and therefore ellipticity. The substitution of all these stages is under way.

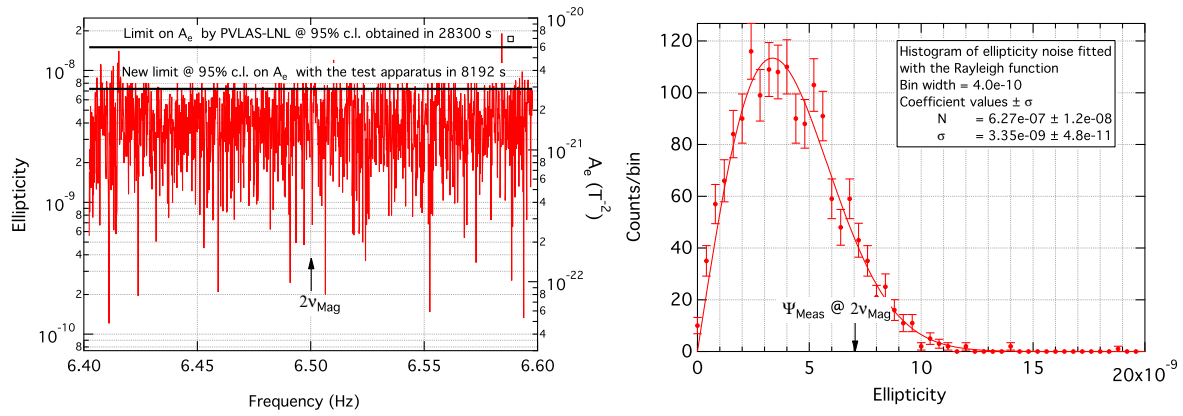

Figure 6. Left: ellipticity noise spectrum in a 0.20 Hz frequency band around $2\nu_{\rm Mag}$. The spectrum is demodulated with a lock-in amplifier with respect to the $\nu_{\rm Mod}$ carrier. The integration time was $T = 8192$ s. Right: histogram of the ellipticity noise values plotted above. A fit with the Rayleigh distribution is superimposed with an ellipticity standard deviation $\sigma = 3.35 \times 10^{-9}$. The arrow indicates the value of the ellipticity Fourier spectrum at exactly $2\nu_{\rm Mag} = 6.5$ Hz.

3.3.3. Noise floor measurements With the test apparatus in a condition in which the peak at $2\nu_{\rm Mag}$ was not present, measurements of a few hours have been done. The magnet rotation frequency was $\nu_{\rm Mag} = 3.25$ Hz. In the left panel of Figure 6 we report the 1600 bin amplitude Fourier noise spectrum of the ellipticity in a frequency band of 0.20 Hz (precisely 1600 bins/8912 s) centred at $2\nu_{\rm Mag}$ for the best measurement; phase information is not reported. The total integration time was 8192 s acquired in a single time record.

In the right panel of the figure, a 50 bin histogram of the same data is given. A vertical arrow in the same figure indicates the ellipticity value of the Fourier spectrum bin at exactly $2\nu_{\rm Mag} = 6.5$ Hz. The probability density function for a noise signal with equal standard deviations σ for the 'in phase' and quadrature components is the Rayleigh function: $P(r) = N\frac{r}{\sigma^2}e^{-\frac{r^2}{2\sigma^2}}$. A fit with the Rayleigh function is superimposed to the histogram. The resulting ellipticity standard deviation is $\sigma = 3.35 \times 10^{-9}$ which translates, at 95% c.l., in a birefringence limit induced by the magnetic field of ($\mathcal{F} = 240000, \lambda = 1064$ nm, $L = 0.4$ m)

$$\Delta n < \sqrt{-2\ln(1-0.95)}\,\frac{\sigma\lambda}{2\mathcal{F}L} = 4.5 \times 10^{-20}. \tag{32}$$

The limits obtained for the parameter A_e and the photon-photon total elastic scattering cross section (at 95 % c.l.) are:

$$A_e < \frac{\Delta n}{3\langle B^2_{\rm ext}\rangle} = 2.45\,\frac{\sigma\lambda}{6\mathcal{F}\int B^2_{\rm ext}\,dL} = 3.3 \times 10^{-21}\ {\rm T}^{-2} \tag{33}$$

$$\sigma_{\gamma\gamma} < 1.2 \times 10^{-62}\ {\rm m}^2\ @\ 1064\ {\rm nm} \tag{34}$$

4. Other experimental efforts

Three other experiments aimed at studying vacuum magnetic birefringence exist: the Q & A experiment, the BMV experiment and the OSQAR experiment. All of them study the propagation of a laser beam through a magnetic field region and use a Fabry-Perot interferometer to increase the optical path length. A number of other proposals have been put forward

to measure vacuum magnetic birefringence [27, 15, 26] or other related quantities [28] with different techniques: they will not be described here. As far as the OSQAR experiment [18] is concerned, the information available in the literature at the time this article was written was rather incomplete.

Vacuum magnetic birefringence appears not only in QED but in a number of different theories. In the case of the Euler-Heisenberg-Weisskopf Lagrangian discussed here, Δn is proportional to $B^2_{\rm ext}$ through the parameter $A_e = \Delta n/(3B^2_{\rm ext})$. On the other hand, the optical quantity the experiments are measuring is the ellipticity generated by the induced birefringence. The relation between birefringence and ellipticity is given in formula (13). The three experiments have therefore two distinct parts: the magnetic field source to generate the birefringence and the optical ellipsometer to measure the induced ellipticity. Figures of merit for the optical setup are the ellipticity sensitivity s at the frequency of interest, the signal amplification factor defined by the Fabry-Perot cavity finesse and the wavelength used.

Table 2. Main parameters of the three ongoing experiments to measure vacuum magnetic birefringence. Effect modulation frequency $f_{\rm mod}$ is $2\nu_{\rm Mag}$ for PVLAS and Q & A, and $1/T_{\rm pulse}$ for BMV.

Experiment	PVLAS	Q & A	BMV
Status	Achieved/Planned	Achieved/Planned	Achieved/Planned
Wavelength (nm)	1064	1064/532	1064
Magnetic dipole	permanent	permanent	pulsed
$\int B^2\,dL$ (T^{2}m)	1.85/10	3.2/19	25/600
Average $B_{\rm ext}$ (T)	2.15/2.5	2.3/2.3	14/30
Finesse	$2.4\times10^5/>4\times10^5$	$3\times10^4/1\times10^5$	$5\times10^5/1\times10^6$
QED ellipticity (Eq. 13)	$3\times10^{-12}/3\times10^{-11}$	$7\times10^{-13}/3\times10^{-11}$	$9\times10^{-11}/5\times10^{-9}$
Detection scheme	heterodyne	heterodyne	homodyne
Effect mod. freq. $f_{\rm mod}$	6 Hz/20 Hz	26 Hz	500 Hz
Duty cicle D_t	~ 1	~ 1	3×10^{-6}
s @ $f_{\rm mod}$ (Hz$^{-1/2}$)	$3\times10^{-7}/3\times10^{-8}$	$1\times10^{-6}/1\times10^{-8}$	$5\times10^{-8}/7\times10^{-9}$
$s_{\rm eff}$ @ $f_{\rm mod}$ (Hz$^{-1/2}$)	$3\times10^{-7}/3\times10^{-8}$	$1\times10^{-6}/1\times10^{-8}$	$3\times10^{-5}/4\times10^{-6}$
$\Delta n_{\rm eff}$ sensitivity (Hz$^{-1/2}$)	$1.7\times10^{-18}/2.5\times10^{-20}$	$3.0\times10^{-17}/7.4\times10^{-21}$	$2.6\times10^{-16}/3.0\times10^{-18}$
$A_{\rm e}$ sensitivity (T^{-2}Hz$^{-1/2}$)	$1.2\times10^{-19}/1.3\times10^{-21}$	$1.8\times10^{-18}/4.7\times10^{-22}$	$4.4\times10^{-19}/1.1\times10^{-21}$
Time for SNR = 1	260 yr/12 d	63×10^3 yr/1.4 d	3.6×10^3 yr/8.3 d

In Table 4 the main features of the ongoing experiments are summarised with an estimated running time necessary to reach the goal of measuring $A_{\rm e}$. As the scheme of the Q & A experiment [17] closely resembles PVLAS's one, the interpretation of its parameters is straightforward. The BMV experiment deserves a few more words: it employs an intense pulsed magnetic field lasting $T_{\rm pulse} = 2$ ms FWHM (total duration about 4 ms), with a repetition rate of five shots per hour to allow the magnets to cool down. Therefore on average the effective duty cycle with the magnetic field ON is $D_t = 2\ {\rm ms} \times (5/3600\ {\rm s}) \approx 3\times10^{-6}$. The analysis correlates the measured ellipticity during each pulse, assumed to be proportional to $B^2_{\rm ext}$, with the magnetic pulse shape, also taking into account the dynamical response of the Fabry-Perot whose decay time is of the order of the magnetic pulse rise time [29]. The analysis gives $\Delta n_{\rm B} = \Delta n/B^2_{\rm filtered}$ for each pulse, where $B_{\rm filtered}$ is the effective field filtered by the first order response of the Fabry-Perot cavity. The BMV collaboration therefore presents results in terms of the birefringence per tesla squared per pulse. At present BMV has obtained a best $\Delta n_B = 5\times10^{-20}$ T^{-2} per pulse and claims that a future upgrade will allow them to reach SNR = 1 in the QED measurement with 1000 pulses [29]. Given a number of pulses $N_{\rm pulses}$ with equivalent noise, the limit on $\Delta n_{\rm B}$ will scale with $1/\sqrt{N_{\rm pulses}}$. In the detection of a birefringence much smaller than $\Delta n_{\rm B}$ many pulses will be needed and therefore, to compare their method with the Q & A or PVLAS capability, it is reasonable to rescale $\Delta n_{\rm B}$ per pulse to the average sensitivity in Δn achievable

in 1 s: $\Delta n_{\rm eff} = \Delta n_{\rm B} B_{\rm ext}^2 \sqrt{T_{\rm pulse}/D_t}$. Since BMV has a small duty cycle D_t their effective optical sensitivity reduces to $s_{\rm eff} = s/\sqrt{D_t}$.

It is apparent that all the experiments are still far from their goal, the chance of their eventual success relying on improvements of the optical sensitivity that, unlike hardware upgrades, cannot be given for granted, as they would require complete understanding of the noise sources limiting the sensitivity. Indeed the shot noise limited sensitivity of all the experiments, given by formula (27), is about a factor between 10 to 100 below the current achieved sensitivities. No clear explanation to this discrepancy has yet been given by any of the collaborations. Note that the best value of sensitivity in ellipticity in ellipsometers using high finesse Fabry-Perot interferometers has been reported by PVLAS in a small test ellipsometer without the implementation of a magnetic field [22] of 2×10^{-8} Hz$^{-1/2}$ above 5 Hz. The best reported sensitivity of a complete apparatus is by BMV with a sensitivity of 5×10^{-8} Hz$^{-1/2}$ over a time span of 2 ms. If in Table 4 the QED ellipticity planned by each experiment is combined with the presently *achieved* sensitivities, the last line in the table would become (3.2, 39, 1.5) years for the three experiments, respectively, instead of (12, 1.4, 8.3) days.

5. Conclusions

We have presented the main physics goal of the PVLAS experiment and have briefly discussed the experimental method. Noise sources are being studied on a bench-top small test apparatus in Ferrara, Italy, in view of the construction of the final apparatus with which we hope to measure for the first time the magnetic birefringence of vacuum due to vacuum fluctuations.

We have discussed the importance, when using rotating magnets, of using not one but two dipole magnets whose relative directions can be made perpendicular to each other in order to have a zero effect condition with the magnetic field present. This is vital to study and eliminate spurious signals generated by the rotating field.

Noise floor measurement results have been presented. A new limit on the parameter A_e describing non linear electrodynamic effects in vacuum has been obtained: $A_e < 3.3 \times 10^{-21}$ T^{-2}. This value, obtained by using two small compact permanent magnets, improves the previous limit by a factor 2.

Finally, the perspectives of the three current existing experimental efforts based on similar techniques active on this subject have been discussed and the experiments compared. Ellipticity noise sources are under study by all groups so as to improve their optical sensitivity. Without such improvements the measurement of vacuum magnetic birefringence is still out of reach.

References

[1] Euler H and Kochel B 1935 *Naturwiss.* **23** 246; Heisenberg W and Euler H 1936 *Z. Phys.* **98** 718; Weisskopf V S 1936 *Kgl. Danske Vid. Sels., Math.-fys. Medd.* **14** 6
[2] Schwinger J 1951 *Phys. Rev.* **82** 664
[3] Baier R and Breitenlohner P 1967 *Acta Phys. Austriaca* **25** 212; Baier R and Breitenlohner P 1967 *Nuovo Cimento* **47**, 261; Adler S L 1971 *Ann. Phys.* **67** 559; Bialynicka-Birula Z and Bialynicki-Birula I 1970 *Phys. Rev. D* **2** 2341
[4] Iacopini E and Zavattini E 1979 *Phys. Lett. B* **85** 151
[5] De Tollis B 1965 *Nuovo Cimento* **35** 1182; De Tollis B 1964 *Nuovo Cimento* **32** 757
[6] Karplus R *et al* 1951 *Phys. Rev.* **83** 776
[7] Dicus D A *et al* 1998 *Phys. Rev. D* **57** 2443
[8] Bernard D *et al* 2000 *Eur. Phys. J. D* **10** 141
[9] Moulin F *et al* 1996 *Z. Phys. C* **72** 607
[10] Bakalov D *et al* 1998 *Hyperfine Interactions* **114** 103; Bakalov D *et al* 1998 *Quantum Semicl. Opt.* **10** 239
[11] Zavattini E *et al* 2008 *Phys. Rev. D* **77** 032006
[12] Bregant M *et al* 2008 *Phys Rev. D* **78** 032006
[13] Lundström *et al* 2006 *Phys. Rev. Lett.* **96** 083602
[14] Tommasini D *et al* 2008 *Phys. Rev. A* **77** 042101

[15] Luiten A N and Petersen J C 2004 *Phys. Lett. A* **330** 429; Luiten A N and Petersen J C 2004 *Phys. Rev. A* **70** 033801
[16] Battesti R *et al* 2008 *Eur. Phys. J. D* **46** 323
[17] Ni W-T 1996 *Chinese J. Phys.* **34** 962
[18] Pugnat P *et al* 2005 Czech. J. Phys. **55** A389
[19] Heinzl T *et al* 2006 *Optics Comm.* **267** 318
[20] Zavattini G *et al* 2012 *Int. J. Mod. Phys. A* **27** 1260017-1
[21] Cameron R *et al* 1993 *Phys. Rev. D* **47** 3707
[22] Della Valle F *et al* 2010 *Optics Comm.* **293** 4194
[23] Jones R C 1948 *J. Opt. Soc. Am.* **38** 671; Hecht E 1987 *Optics* 2nd ed. (San Francisco: Addison-Wesley)
[24] Zavattini G *et al* 2006 *Appl. Phys. B* **83** 571
[25] Ruoso G and Zavattini G 1996 *Proceedings of the Seventh Marcel Grossman Meeting* Jantzen R T and Mac Kaiser G eds. (Singapore: World Scientific) p 1379; Cantatore G *et al* 1995 *Rev. Sci. Instrum.* **66** 2785
[26] Zavattini G and Calloni E 2009 *Eur. Phys. J. C* **62** 459
[27] Hall J L *et al* 2000 *Phys Rev. A* **62** 013815
[28] Partovi M H 1993 *Preprint* hep-ph/9308293v1
[29] Berceau P *et al* 2012 *Phys. Rev. A* **85** 013837